IRIS AperTO

UNIVERSITÀ DEGLI STUDI DI TORINO

AperTO - Archivio Istituzionale Open Access dell'Università di Torino

A new eight-cation inverse high entropy spinel with large configurational entropy in both tetrahedral and octahedral sites: Synthesis and cation distribution by X-ray absorption spectroscopy

This is the author's manuscript

Original Citation:

Availability:

This version is available http://hdl.handle.net/2318/1770204 since 2021-01-30T19:12:08Z

Published version:

DOI:10.1016/j.scriptamat.2020.07.002

Terms of use:

Open Access

Anyone can freely access the full text of works made available as "Open Access". Works made available under a Creative Commons license can be used according to the terms and conditions of said license. Use of all other works requires consent of the right holder (author or publisher) if not exempted from copyright protection by the applicable law.

(Article begins on next page)

07 January 2023

A new eight-cation inverse high entropy spinel with large configurational entropy in both tetrahedral and octahedral sites: synthesis and cation distribution by X-ray absorption spectroscopy

Martina Fracchia*[a], Maela Manzoli[b], Umberto Anselmi-Tamburini[a,c], Paolo Ghigna[a,c]

[a] *Department of Chemistry, University of Pavia, Via T. Taramelli 12, 27100 Pavia, Italy*

[b] *Department of Drug Science and Technology and NIS - Centre for Nanostructured Interfaces and Surfaces, Via P. Giuria 9, 10125 Turin, Italy*

[c]*INSTM, National Inter-University Consortium for Materials Science and Technology, Via G. Giusti 9, 50121 Florence, Italy*

*Corresponding author

Mail address: martina.fracchia02@universitadipavia.it

Postal address: Department of Chemistry, University of Pavia, Via Taramelli 12, 27100 Pavia, Italy

Abstract

In this work we report the synthesis of $(Co,Mg,Mn,Ni,Zn)(Al,Co,Cr,Fe,Mn)_2O_4$ in a single-phase spinel structure (space group $Fd\bar{3}m$). The chemical homogeneity and purity of the sample were checked through X-ray diffraction, high resolution transmission electron microscopy and energy dispersive X-ray spectroscopy. The analysis of the pre-edge peaks of the X-ray absorption spectra for all the transition metals clearly indicated the presence of a partial degree of inversion in the spinel structure. This material is characterized by a particularly large configurational entropy, regarding both the A and the B sites, leading to a total value equal to 3.3 in R unit.

Keywords: high entropy oxides; spinels; configurational entropy; inversion

In the recent years, the concept of high entropy has been explored in numerous classes of materials, ranging from high entropy alloys (HEAs)[1], to high entropy carbides (HECs) [2], borides (HEBs)[3], and to high entropy oxides (HEOs)[4]. In high entropy alloys, at least 5 components are mixed in a near-equimolar quantity, resulting into a single-phase structure where the large value of configurational entropy leads to unusual and unique properties [5,6]. The possibility to extend this same concept for the synthesis of oxides has first been considered in a pioneering work by Rost *et al.* in 2015 [4], where CuO, CoO, MgO, NiO and ZnO were mixed together in equimolar ratio and heated up to 900 °C resulting into single-phase $(Co_{0.2}Cu_{0.2}Mg_{0.2}Ni_{0.2}Zn_{0.2})O$ with a rock-salt structure. It should be noted that not all the corresponding parent compounds are stable in the rock-salt structure at ambient pressure and room temperature: CuO has a

monoclinic structure, where Cu is in a highly distorted octahedral geometry. The stabilization of CuO in a perfect cubic geometry is, in fact, strongly hindered by the Jahn Teller contribution, particularly large in the case of d^9 electronic configuration. Analogously, ZnO is usually stable in the wurtzite structure. The possibility of stabilizing all these binary compounds into a single rock-salt phase is a direct effect of the value of the configurational entropy, exceptionally large in case of a multicomponent (generally up to 5 components) equimolar mixture, which compensates for the unfavourable correspondent enthalpic contribution.

The seminal work by Rost raised much interest in the research community, offering a new paradigm where the so-called *cocktail effect* can lead to the synthesis and design of innovative oxide materials with new physical and structural properties. The same properties of (CoCuMgNiZn)O are currently being investigated, and it has emerged that this material can be promising for future applications in catalysis [7,8] and for energy production and storage, *e.g.*. as anode material in Li-ion batteries [9,10], or as large *k* dielectric material [11]. It is therefore not surprising that the possibility of stabilizing high entropy oxides in crystal structures other than the rock-salt has immediately attracted great attention. The possibility of obtaining high-entropy perovskite oxides was reported by Jiang *et al.* [12] while, concurrently, Sarkar *et al.* could synthetize for the first time a pure 10-cationic high entropy oxide in the perovskite phase, namely $(Gd_{0.2}La_{0.2}Nd_{0.2}Sm_{0.2}Y_{0.2})(Co_{0.2}Cr_{0.2}Fe_{0.2}Mn_{0.2}Ni_{0.2})O_3$ [13]. High entropy fluorites oxides and pyrochlore oxides were also reported[14,15]. The first high entropy oxide with spinel structure, $(Co,Cr,Fe,Mn,Ni)_3O_4$, was obtained in 2018 [16], and other possible cation combinations have very recently appeared in literature [17–19]. It is well known that spinels dominate the field of materials chemistry, having many applications ranging from magnetism [20] to anodes/cathodes for Li and Na-ion batteries [21–23], catalysis [24] and many others.

The spinel phase has general formula AB_2O_4: in the so-called normal spinels, A is a bivalent cation, occupying tetrahedral sites, while B is a trivalent cation occupying the octahedral sites. In this work, we report for the first time the synthesis of the single-phase 8-cation high entropy spinel $(Co_{0.2}Mg_{0.2}Mn_{0.2}Ni_{0.2}Zn_{0.2})(Al_{0.2}Co_{0.2}Cr_{0.2}Fe_{0.2}Mn_{0.2})_2O_4$, where both the A site and the B site are occupied by 5 cations and are therefore characterized by an unprecedented high value of configurational entropy for a spinel phase.

The HE spinel was obtained via solid-state reaction starting from the correspondent oxides (the details can be found in the Supplementary Information); the oxides were mixed in an agar mortar and treated at 1200 °C (10 °C/min ramp rate) for 6 hours and quenched to room temperature. A single-phase HE was then obtained after a further treatment at 1500 °C (10 °C/min ramp rate) for 6 hours. The sample was first characterized by X-ray diffraction (XRD) using a D8 Advance diffractometer (Bruker) with Cu Kα radiation and by Scanning Electron Microscopy (SEM) and checked for chemical homogeneity by Energy Dispersive X-ray Spectroscopy (EDS). These measurements were performed using a Tescan Mira3XMU microscope operating at 20 kV and equipped with an EDAX EDS analysis system; the sample was impregnated by epoxy resin, polished with finer grained abrasive paper and then coated with a carbon thin film using a Cressington

208carbon coater. The XRD diffraction pattern is shown in Fig. 1a. The pattern confirms the formation of a single phase, where all the visible reflections can be attributed to the spinel structure (space group $Fd\bar{3}m$). The lattice constant was found to be a = 8.3207 (±0.001) Å (more details can be found in the Supplementary Information). The SEM and the EDS analysis, shown in Fig. 1b, demonstrated the homogeneity of the sample on the micrometric scale from both a structural and a chemical point of view.

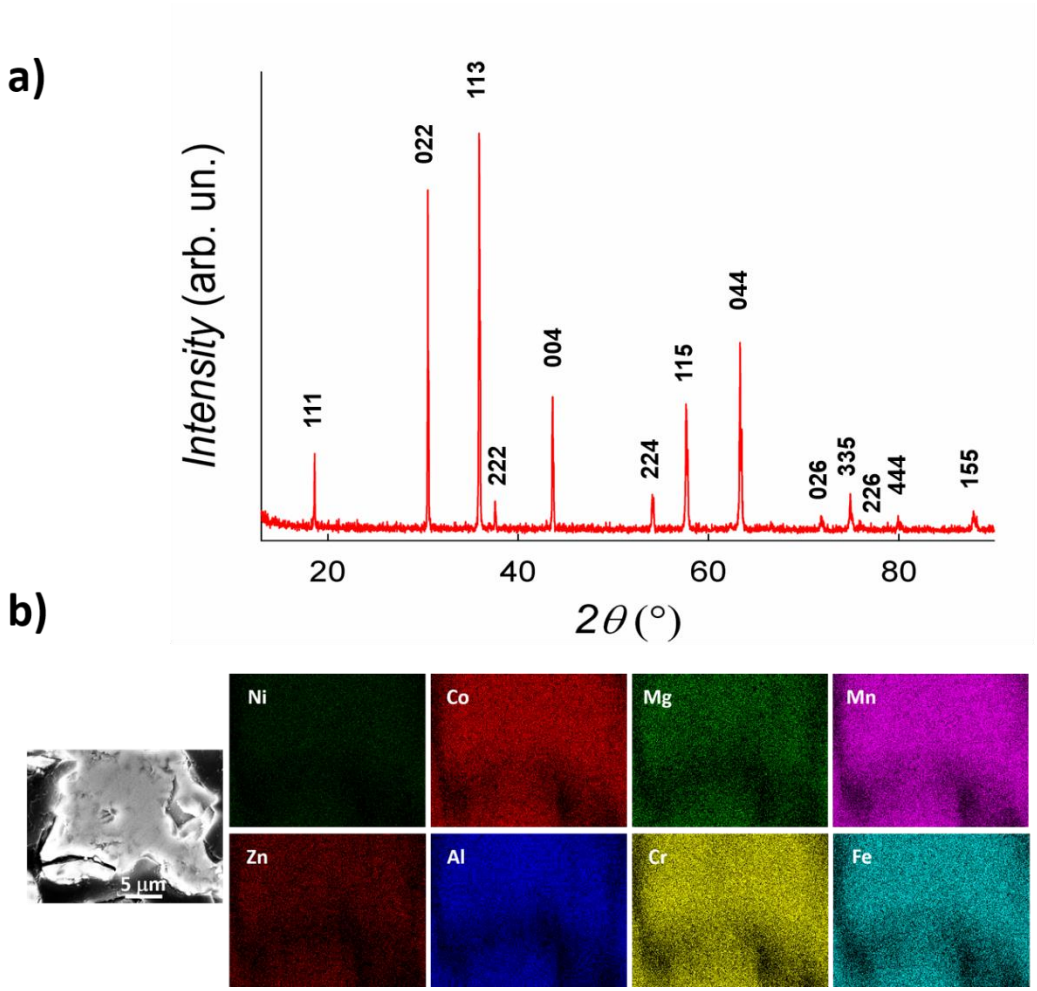

Fig. 1: a) X-ray diffraction pattern of $(Co,Mg,Mn,Ni,Zn)(Al,Co,Cr,Fe,Mn)_2O_4$ synthetized as described in the main text. All the reflections can be indexed according to the spinel phase (space group $Fd\bar{3}m$). b) EDS maps for all the 8 cations in the spinel phase; the uniformity of all the maps shows that the sample is chemically homogeneous.

The morphology and the crystalline and chemical homogeneity of the material were further investigated by transmission electron microscopy (TEM, see Fig. S1 in the Supplementary Information), high resolution TEM (HR-TEM) and field emission (FE) SEM (for more details refer to the Supplementary Information). The TEM measurements were performed using a side entry Jeol JEM 3010 (300 kV) microscope equipped with a LaB_6 filament and fitted with X-ray EDS analysis by a Link ISIS 200 detector. For analyses, the powdered samples were deposited on a copper grid, coated with a porous carbon film. All digital

micrographs were acquired using an Ultrascan 1000 camera and the images were processed by Gatan digital micrograph. It is worth noting that the synthetized (Co,Mg,Mn,Ni,Zn)(Al,Co,Cr,Fe,Mn)$_2$O$_4$ sample proved to be stable to prolonged exposition under the electron beam of the instrument. A representative HR-TEM image of the spinel is shown in Fig. 2a, where the Fourier Transform of the image reported in Fig. 2b, as well as the presence of diffraction fringes with spacing typical of the (113) plane of the cubic phase (Fig. 2c), indicate uniform crystallinity of the whole region. Moreover, the EDS analysis demonstrated the homogeneous distribution of the different elements within the mapped region also at high magnification (Fig. 2d and 2e), which points out an extremely uniform distribution of the cations in the material from both micro- and nanometric scales (additional experimental evidences have been reported in Figs. S3 and S4 of the Supplementary Information). The EDS spectrum of the zone shown in Figure 2a is reported in the Supplementary Information (Fig. S5). The results of the FESEM characterization (summarized in the Supplementary Information, Figs. S6-S9) further corroborate these findings.

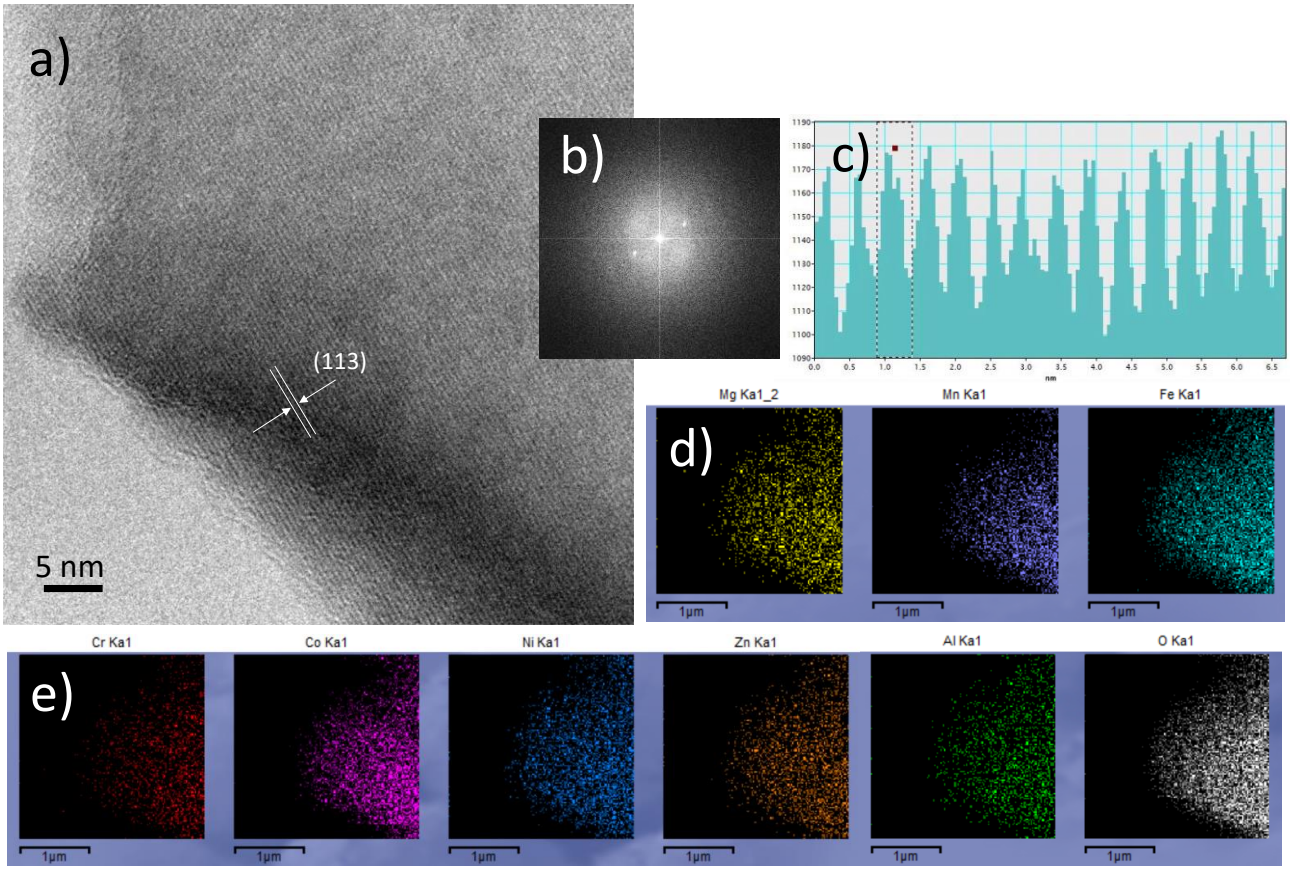

Fig. 2: a) HR-TEM image of (Co,Mg,Mn,Ni,Zn)(Al,Co,Cr,Fe,Mn)$_2$O$_4$. b) Fourier Transform of the image in a). c) Measure of the spacing between the diffraction fringes observed in the zone of the sample shown in a). d) and e) EDS maps of the region shown in a) for all the 8 cations and oxygen in the spinel phase. Instrumental magnification: 400000×.

It is well known that spinels can exist in either normal or inverse structure; while the EDS gives information on the homogeneity of the sample, no information is given about the cation distribution. For a more detailed investigation on the structural and electronic properties of each transition metal in the spinel phase, X-ray Absorption Spectroscopy (XAS) measurements were performed at the Co, Mn, Ni, Zn, Fe and Cr K-edge (see Fig. 3); all the measurements were done at the XAFS beamline of the ELETTRA synchrotron radiation facility. For 3*d* transition metals, the so-called pre-edge peaks are particularly informative and allow discriminating between different coordination geometries by a brief analysis of their intensity and shape [25,26]. The pre-edge peaks are small features at the base of the main edge in the XAS spectrum and result from the dipole forbidden transition from filled 1*s* orbitals to empty 3*d* orbitals.

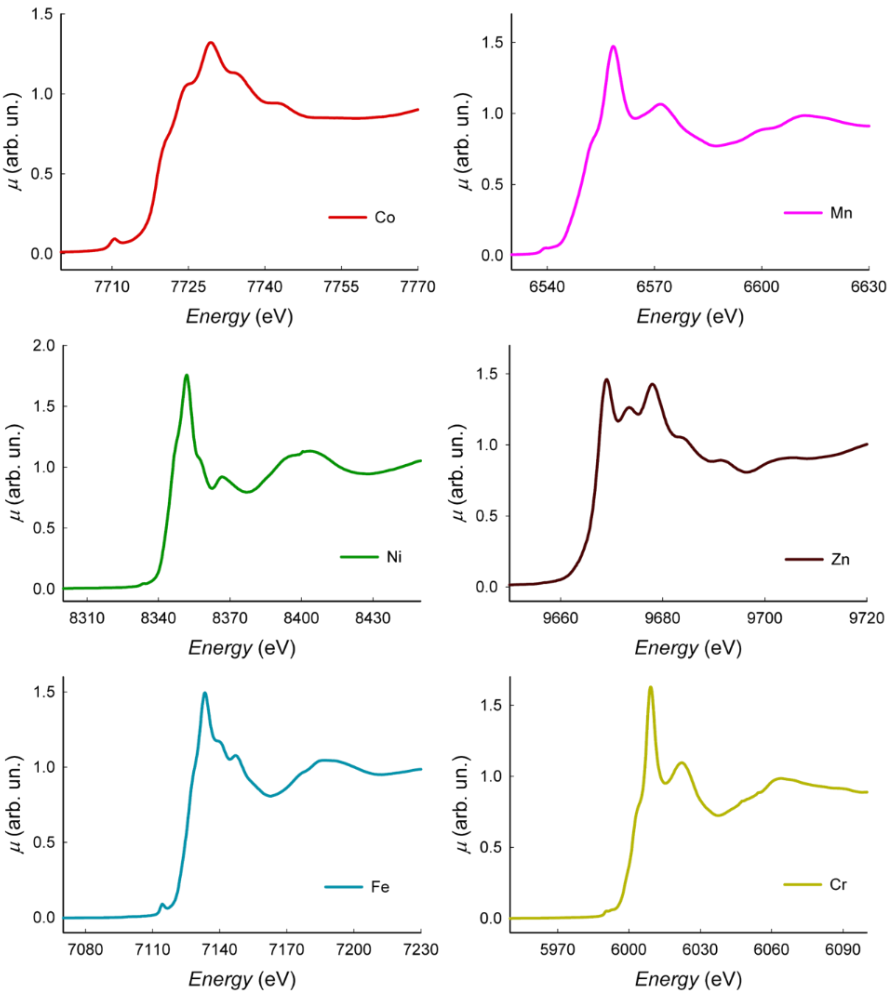

Fig. 3: XAS spectra of (Co,Mg,Mn,Ni,Zn)(Al,Co,Cr,Fe,Mn)$_2$O$_4$ at the Co, Mn, Ni, Zn, Fe and Cr K-edge.

The pre-edge peaks of metals in perfect octahedral coordination display a very low intensity ($\mu \sim$ 0.1-0.2), having only a quadrupolar nature. In case of other coordination geometries (*e.g.* tetrahedral, distorted octahedral *etc.*), the lack of the inversion centre leads to a partial hybridization between *d* and *p* orbitals: since the transition to orbitals of *p* symmetry is dipole allowed, the resulting peaks usually have a higher

intensity. The pre-edge peaks were extracted and background-subtracted for each absorption edge and are shown in Fig. 4. More details on data acquisition and treatment can be found in the Supplementary Information; here we note that to obtain more accurate information on the local chemical environment of the transition metals, the pre-edge peak was fitted with the minimum number of Gaussians. According to the expected stoichiometry (Co,Mg,Mn,Ni,Zn)(Al,Co,Cr,Fe,Mn)$_2$O$_4$, cobalt and manganese should occupy both tetrahedral and octahedral sites. If we look at the pre-edge region at the Co K-edge in Fig. 4, it can be seen that it is dominated by an intense peak, slightly asymmetric at higher energies. This peak was therefore fitted with two Gaussian functions: one of higher intensity, centred at 7110.4 eV, that accounts for an allowed dipole-transition with cobalt in the tetrahedral coordination, and one of much lower intensity, 2 eV above, accounting for Co^{3+} in an octahedral environment.

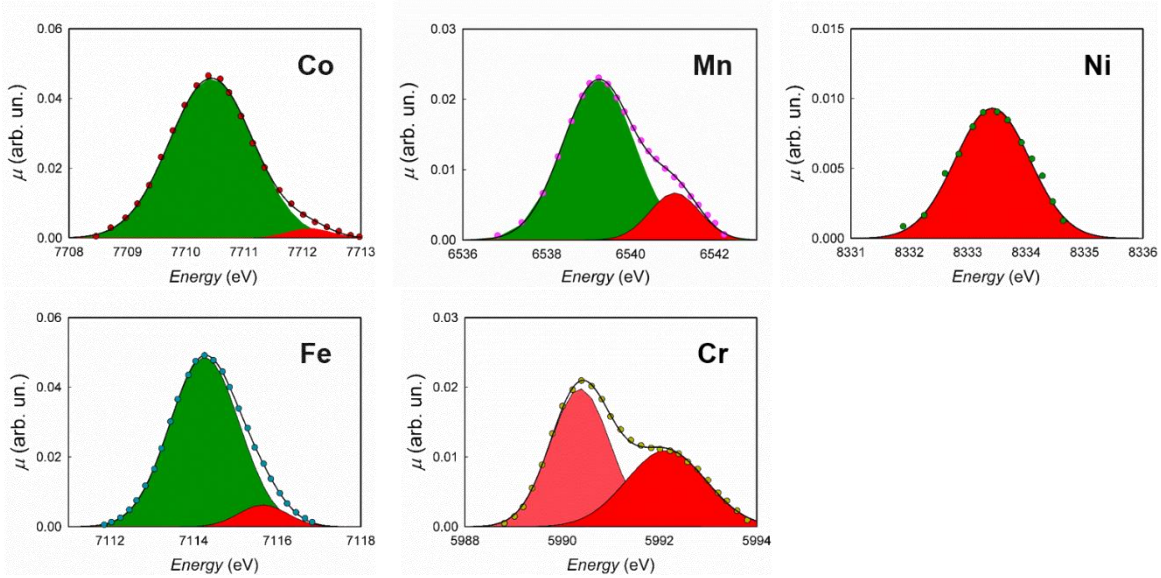

Fig. 4: Pre-edge peaks obtained after background subtraction at the Co, Mn, Ni, Zn, Fe and Cr K-edge. The dotted lines represent the experimental curve, while the black solid line is the resulting fit, obtained with the corresponding Gaussian functions (the green Gaussian peaks correspond to the 1*s* →3*d* transition in case of tetrahedrally coordinated metals, while the red ones are in case of octahedrally coordinated metals).

It should be noted that this last transition should result into two distinct peaks, due to the electronic transition from 1*s* to empty 3*d* orbitals with t_{2g} or e_g symmetry, respectively. However, the t_{2g} peak, at lower energies, is hidden by the first Gaussian and cannot be discerned. The pre-edge region at the Mn K-edge can be simulated in a similar way as for cobalt, with a first Gaussian function at 6539 eV attributed to Mn^{2+} in a tetrahedral coordination and a second Gaussian function (at 6541 eV) for Mn^{3+} in the octahedral sites. In this case, however, the first peak is not the dominating feature and the two peaks are well distinct: this is in agreement with what is expected for Mn in mixed tetrahedral/octahedral sites (for instance, the pre-edge peak at the Mn K-edge of Mn_3O_4 is analogous[27]). The pre-edge profile which is found for Co indicates,

therefore, that differently to what happens for Mn, the A sites are not only occupied by divalent Co, but also partially by Co^{3+}: this clearly suggests the presence of a certain degree of inversion in the HE spinel.

As evident from Fig. 3, the spectrum at the Zn K-edge does not present any pre-edge region, since Zn^{2+} is in electronic configuration $[Ar]3d^{10}$; the spectrum profile is in total agreement with Zn^{2+} occupying A sites, as found, for instance, for $ZnFe_2O_4$ [28]. On the contrary, the pre-edge peak at the Ni K-edge is weak, demonstrating the Ni predominantly occupies the B site; the signal can be efficiently simulated by one Gaussian function which accounts for the only possible transition to e_g orbitals. Finally, according to the expected stoichiometry, Cr and Fe are expected to occupy the B sites. The spectrum at the Cr K-edge presents two weak peaks in the pre-edge region that are characteristic of Cr^{3+} in an octahedral environment and correspond to the two transitions to t_{2g} and e_g orbitals. On the contrary, the pre-edge peaks at the Fe K-edge can be fitted with two Gaussian functions, one of high intensity, related to Fe^{3+} occupying tetrahedral sites, and one of lower intensity related to Fe^{3+} in octahedral sites. Again, the two possible transitions to t_{2g} and e_g orbitals cannot be distinguished.

The above results show that the HE spinel presents a high degree of inversion, where Ni ions preferentially occupies the B sites, Fe occupies both A and B sites and Co ions are predominantly found in the A sites. This is not surprising, considering that both $NiFe_2O_4$ and $NiCo_2O_4$ are usually found with an inverse spinel structure at room temperature and atmospheric pressure [29–31], while $CoFe_2O_4$ often shows a partial degree of inversion under the same conditions [30]. In summary, the above data allow assessing the location of Cr and Ni in the octahedral site, of Zn in the tetrahedral site and mixed location for Mn, Fe and Co. By assuming that Al occupies only the octahedral site, while Mg is located in the tetrahedral site only, and recalling the original stoichiometry, we can obtain a sensible evaluation of the site distribution of the present spinel as $(Mg_{0.2}Mn_{0.2}Zn_{0.2}Fe_{0.1}Co_{0.3})^{T}(Al_{0.2}Cr_{0.2}Mn_{0.2}Fe_{0.15}Co_{0.15}Ni_{0.1})_2^{O}O_4$. With this chemical formula, and applying the following equation:

$$S_{config} = -R\left(\sum_{i,T}^{n_T} \chi_{i,T} ln\chi_{i,T} + \sum_{i,O}^{n_O} \chi_{i,O} ln\chi_{i,O}\right)$$

where χ_i are the molar fraction and *T* and *O* refer to the tetrahedral and octahedral sites, respectively, we obtain a figure of 3.3*R* for the configurational entropy in this spinel, which is more than the double compared to 1.5*R*, considered the lower limit for the so called high entropy compounds [32] .

To conclude, in this study we reported the synthesis of the inverse high entropy $(Co,Mg,Mn,Ni,Zn)(Al,Co,Cr,Fe,Mn)_2O_4$ spinel. This material presents an unprecedented high value of the configurational entropy for both the A and B site of the spinel structure: this is expected to have a strong influence in several physical properties, *e.g.* in magnetic and catalytic properties. In addition, we believe that this material can be a starting point for novel applications in energetics as well as for the investigation and stabilization of other HE spinels with a different range of compositions and/or including different cations.

Moreover, we report the analysis of the pre-edge XAS peaks as a powerful instrument in the field of HEOs, allowing to get specific electronic and structural information on each transition metal in the structure.

Acknowledgements

The ELETTRA synchrotron radiation facility is acknowledged for the provision of beamtime (experiment 20190004). The Authors are thankful to Dr. Danilo Oliveira de Souza for help during the XAS experiment, to Dr. Maria Carmen Valsania for the FESEM measures and to Dr. Andrea Bianchi for his help concerning the SEM measurements. The authors are also thankful to CiSRIC-UNIPV for the SEM analysis. This work has been partially financed by the Italian Ministry of University and Research (MIUR) (grant "PRIN 2017, 2017KKP5ZR, MOSCATo").

References

[1] M. Tsai, J. Yeh, M. Tsai, J. Yeh, Mater. Res. Lett. 2 (2014) 107–123.
[2] J. Zhou, J. Zhang, F. Zhang, B. Niu, L. Lei, W. Wang, Ceram. Int. 44 (2018) 22014–22018.
[3] J. Gild, Y. Zhang, T. Harrington, S. Jiang, T. Hu, M.C. Quinn, W.M. Mellor, N. Zhou, K. Vecchio, J. Luo, Sci. Rep. 6 (2016) 2–11.
[4] C.M. Rost, E. Sachet, T. Borman, A. Moballegh, E.C. Dickey, D. Hou, J.L. Jones, S. Curtarolo, J. Maria, Nat. Commun. 6 (2015) 1–8.
[5] D.B. Miracle, O.N. Senkov, Acta Mater. 122 (2017) 448–511.
[6] Y. Zhang, T. Ting, Z. Tang, M.C. Gao, K.A. Dahmen, P.K. Liaw, Z. Ping, Prog. Mater. Sci. 61 (2014) 1–93.
[7] M. Fracchia, P. Ghigna, T. Pozzi, U. Anselmi Tamburini, V. Colombo, L. Braglia, P. Torelli, J. Phys. Chem. Lett. 11 (2020) 3589–3593.
[8] H. Chen, J. Fu, P. Zhang, H. Peng, C.W. Abney, K. Jie, X. Liu, M. Chi, S. Dai, J. Mater. Chem. A 6 (2018) 11129–11133.
[9] A. Sarkar, L. Velasco, D. Wang, Q. Wang, G. Talasila, L. de Biasi, C. Kübel, T. Brezesinski, S.S. Bhattacharya, H. Hahn, B. Breitung, Nat. Commun. 9 (2018).
[10] Q. Wang, A. Sarkar, Z. Li, Y. Lu, L. Velasco, S.S. Bhattacharya, T. Brezesinski, H. Hahn, B. Breitung, Electrochem. Commun. 100 (2019) 121–125.
[11] D. Bérardan, S. Franger, D. Dragoe, A.K. Meena, N. Dragoe, Phys. Status Solidi - Rapid Res. Lett. 10 (2016) 328–333.
[12] S. Jiang, T. Hu, J. Gild, N. Zhou, J. Nie, M. Qin, T. Harrington, K. Vecchio, J. Luo, Scr. Mater. 142 (2018) 116–120.
[13] A. Sarkar, R. Djenadic, D. Wang, C. Hein, R. Kautenburger, O. Clemens, H. Hahn, J. Eur. Ceram. Soc. 38 (2018) 2318–2327.
[14] J. Gild, M. Samiee, J.L. Braun, T. Harrington, H. Vega, P.E. Hopkins, K. Vecchio, J. Luo, J. Eur. Ceram. Soc. 38 (2018) 3578–3584.
[15] Z. Teng, L. Zhu, Y. Tan, S. Zeng, Y. Xia, Y. Wang, H. Zhang, J. Eur. Ceram. Soc. 40 (2020) 1639–1643.
[16] J. Dąbrowa, M. Stygar, A. Mikuła, A. Knapik, K. Mroczka, W. Tejchman, M. Danielewski, M. Martin, Mater. Lett. 216 (2018) 32–36.
[17] A. Mao, H.Z. Xiang, Z.G. Zhang, K. Kuramoto, H. Zhang, Y. Jia, J. Magn. Magn. Mater. 497 (2020) 1–5.
[18] M. Stygar, J. Dąbrowa, M. Moździerz, M. Zajusz, W. Skubida, K. Mroczka, K. Berent, K. Świerczek, M. Danielewski, J. Eur. Ceram. Soc. 40 (2020) 1644–1650.
[19] T. Parida, A. Karati, K. Guruvidyathri, B.S. Murty, G. Markandeyulu, Scr. Mater. 178 (2020) 513–517.

[20] D.S. Mathew, R.S. Juang, Chem. Eng. J. 129 (2007) 51–65.
[21] D. Liu, W. Zhu, J. Trottier, C. Gagnon, F. Barray, A. Guerfi, A. Mauger, H. Groult, C.M. Julien, J.B. Goodenough, K. Zaghib, RSC Adv. 4 (2014) 154–167.
[22] E. Ferg, R.J. Gummow, A. De Kock, J. Electrochem. Energy Convers. Storage 141 (1994) 9–12.
[23] L. Zhao, H.L. Pan, Y.S. Hu, H. Li, L.Q. Chen, Chinese Phys. B 21 (2012) 4–8.
[24] Q. Zhao, Z. Yan, C. Chen, J. Chen, Chem. Rev. 117 (2017) 10121–10211.
[25] T.E. Westre, P. Kennepohl, J.G. DeWitt, B. Hedman, K.O. Hodgson, E.I. Solomon, J. Am. Chem. Soc. 119 (1997) 6297–6314.
[26] M. Fracchia, A. Visibile, E. Ahlberg, A. Vertova, A. Minguzzi, P. Ghigna, S. Rondinini, ACS Appl. Energy Mater. 1 (2018) 1716–1725.
[27] T.G. Kim, S.J. Kim, C.C. Lin, R.S. Liu, T.S. Chan, S.J. Im, J. Mater. Chem. C 1 (2013) 5843–5848.
[28] M.J. Akhtar, M. Nadeem, S. Javaid, M. Atif, J. Phys. Condens. Matter 21 (2009).
[29] Y. Bitla, Y.Y. Chin, J.C. Lin, C.N. Van, R. Liu, Y. Zhu, H.J. Liu, Q. Zhan, H.J. Lin, C. Te Chen, Y.H. Chu, Q. He, Sci. Rep. 5 (2015) 1–8.
[30] D. Carta, D. Loche, G. Mountjoy, G. Navarra, A. Corrias, J. Phys. Chem. C 112 (2008) 15623–15630.
[31] J.L. Ortiz-Quiñonez, U. Pal, M.S. Villanueva, ACS Omega 3 (2018) 14986–15001.
[32] A. Sarkar, Q. Wang, A. Schiele, M.R. Chellali, S.S. Bhattacharya, D. Wang, T. Brezesinski, H. Hahn, L. Velasco, B. Breitung, Adv. Mater. 31 (2019).

Supplementary Information

Synthesis

Crystalline (Co,Mg,Mn,Ni,Zn)(Al,Co,Cr,Fe,Mn)$_2$O$_4$ was synthetized starting from Co_3O_4, Fe_2O_3, Mn_3O_4, Cr_2O_3, Al_2O_3, NiO, ZnO, MgO. All the reagents were purchased with high purity (> 99.7 %) from Sigma Aldrich. The oxides were weighted in stoichiometric proportion and vigorously grinded with an agar mortar and pestle. The resulting powder was treated at 1200 °C (ramp rate 10 °C/min) for 6 hours and then quenched in air to room temperature. Afterwards, a single-phase spinel with micrometric size was obtained with an additional treatment at 1500 °C for 6 hours (ramp rate 10 °C/min).

X-ray diffraction (XRD)

The diffraction pattern was analysed through the Rietveld method. The average atomic number of the atoms in the A site is 24.4, close to the atomic number of Cr (24); the average atomic number of the atoms in the B site is in turn 23, correspondent to the atomic number of V. Consequently, we decided to simulate the pattern starting from a cubic AB_2O_4 spinel (space group $Fd\bar{3}m$), with Cr occupying the A site and V occupying the B site.

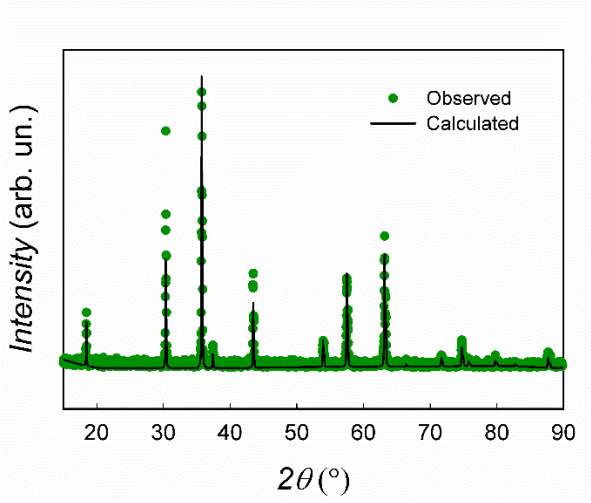

Fig. S1: XRD experimental pattern (green dotted line) and calculated through Rietveld refinement (black solid line).

The goodness of factor of the Rietveld simulation is χ^2 = 12.6. It can be seen from Fig. S1 that all the reflections correspond to the spinel phase. The position of the peaks is also well-determined, and is directly connected to the lattice constant, whose value obtained after the refinement is a = 8.3207 Å. The intensity of the peaks, however, is not very well determined, especially for the reflections at 2θ = 30.5° and 43.5°, which usually present lower intensity in the spinel structure. This is probably due to the inversion degree, which is however difficult to handle due to the complicate formula and to the close atomic number of the major part of the cations.

Transmission electron microscopy (TEM) and high resolution (HR) TEM

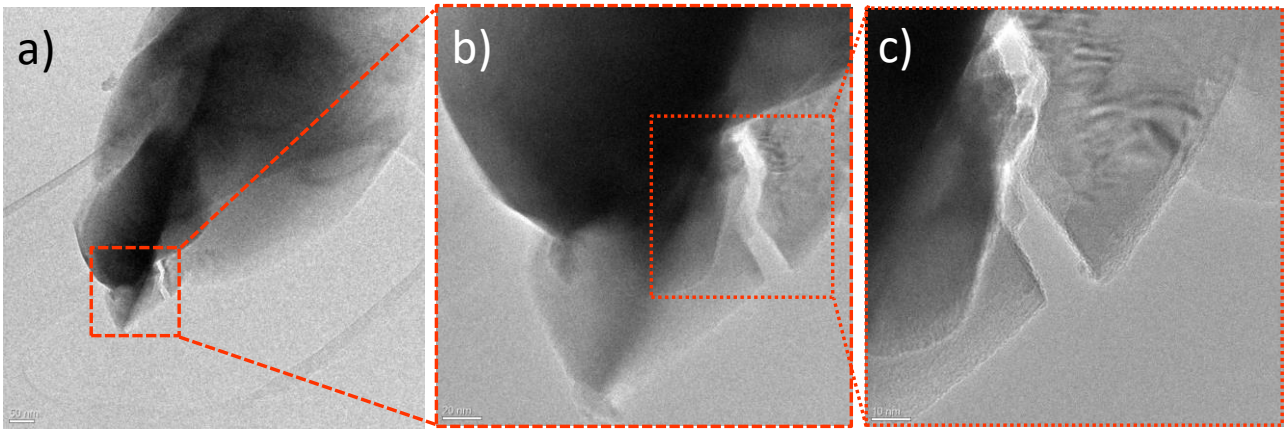

Fig. S2: a) Low magnification TEM image of the (Co,Mg,Mn,Ni,Zn)(Al,Co,Cr,Fe,Mn)$_2$O$_4$ sample. b) zoom of the region highlighted by the orange box in a). c) zoom of the region highlighted by the orange box in b). Instrumental magnification: 25000×, 100000× and 200000×.

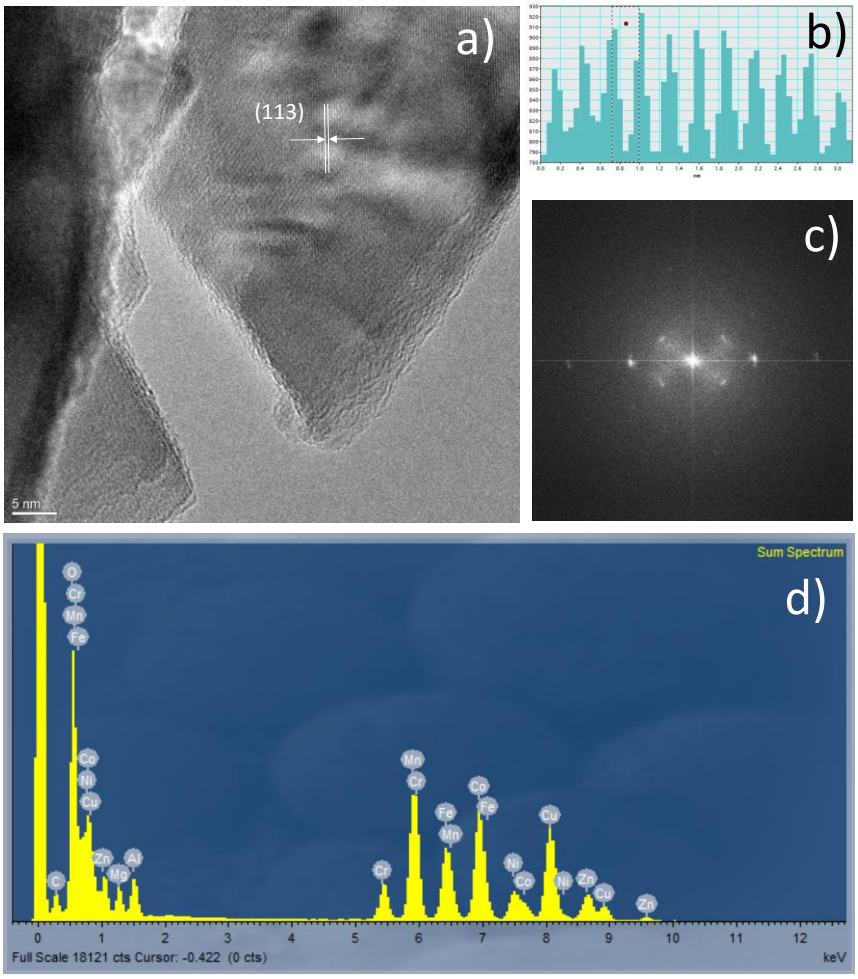

Fig. S3: a) HR-TEM image of (Co,Mg,Mn,Ni,Zn)(Al,Co,Cr,Fe,Mn)$_2$O$_4$. b). Measure of the spacing between the diffraction fringes observed in the zone of the sample shown in a). c) Fourier Transform of the image in a). d) EDS sum spectrum of the HRTEM image shown in a). Instrumental magnification: 400000×.

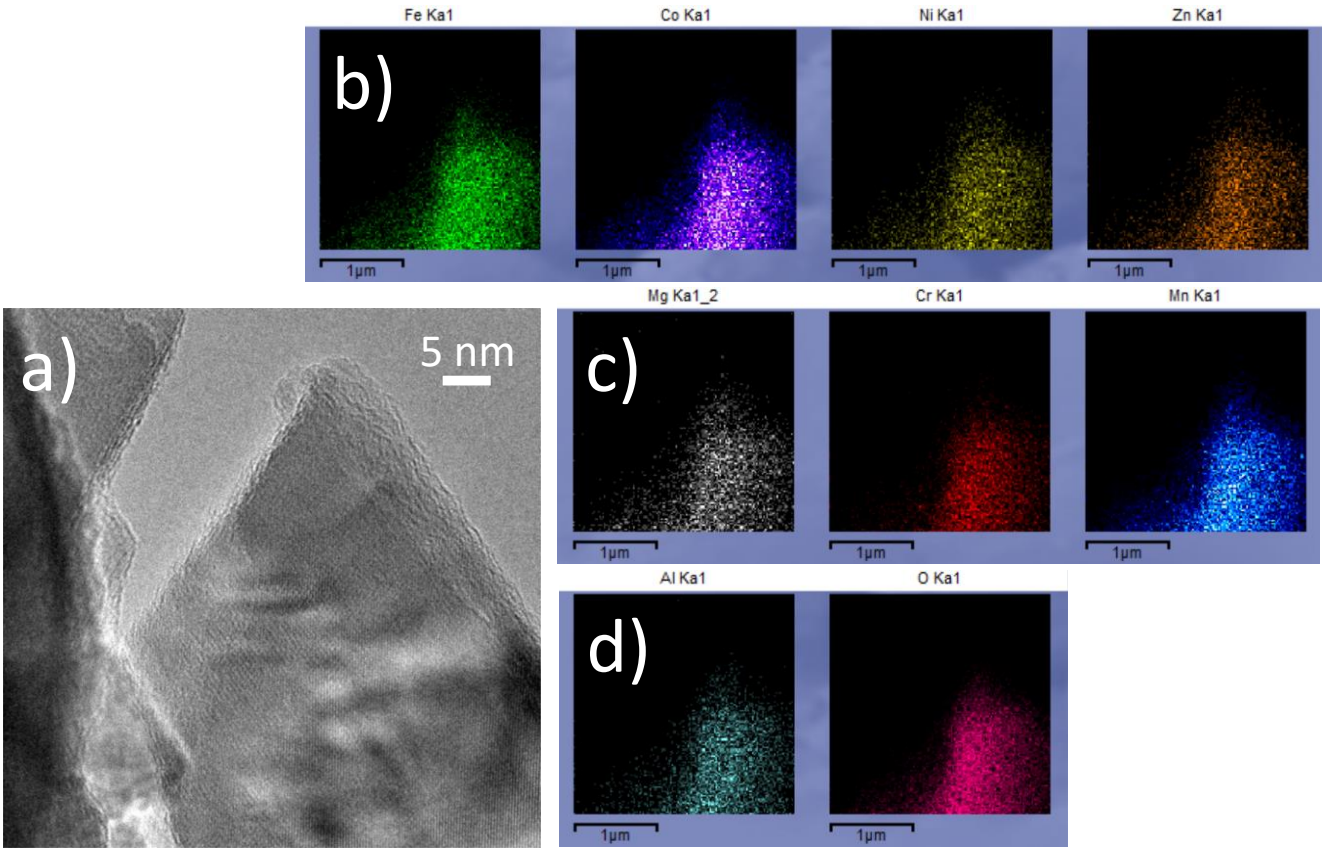

Fig. S4: a) HR-TEM image of (Co,Mg,Mn,Ni,Zn)(Al,Co,Cr,Fe,Mn)$_2$O$_4$. b), c) and d) EDS maps of the region shown in a) for all the 8 cations and oxygen in the spinel phase. Instrumental magnification: 400000×.

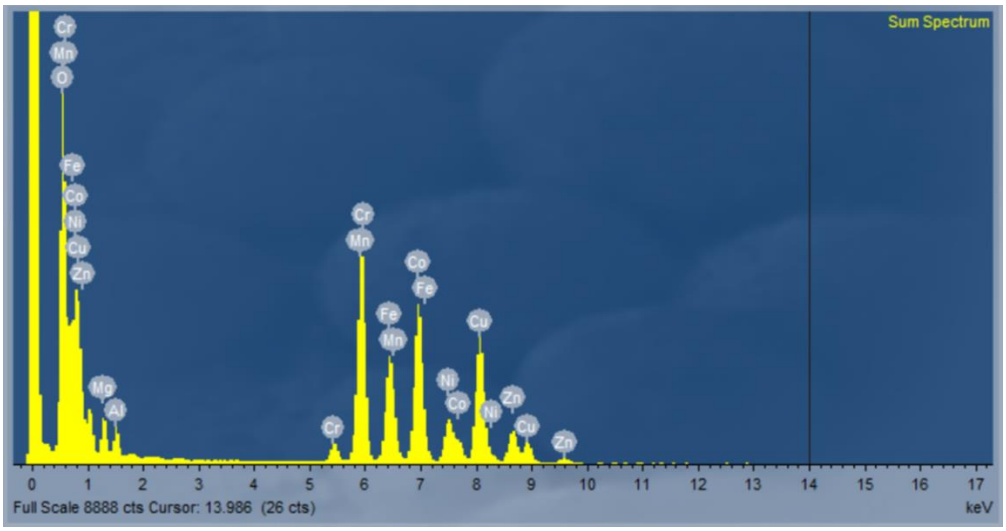

Fig. S5: EDS sum spectrum of the HRTEM image shown in Fig. 2.

Field emission scanning electron microscopy (FESEM)

The FESEM measurements were performed using a Tescan S9000G FESEM 3010 microscope (30 kV) equipped with a high brightness Schottky emitter and fitted with Energy Dispersive X-ray Spectroscopy (EDS) analysis by a Ultim Max Silicon Drift Detector (SDD, Oxford). For analyses, the powdered samples were deposited on a stub and inserted in the chamber by a fully motorized procedure.

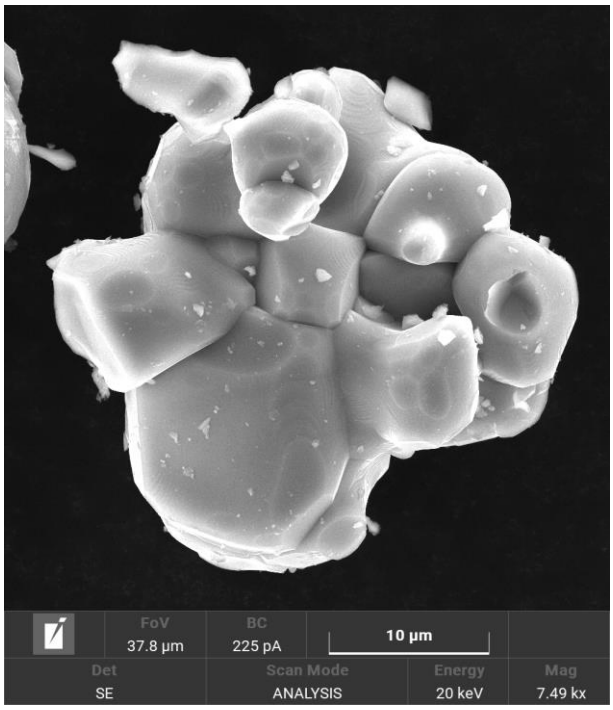

Fig. S6: FESEM image of (Co,Mg,Mn,Ni,Zn)(Al,Co,Cr,Fe,Mn)$_2$O$_4$. Image collected at 20 kV with the standard SE detector. Instrumental magnification: 7490×.

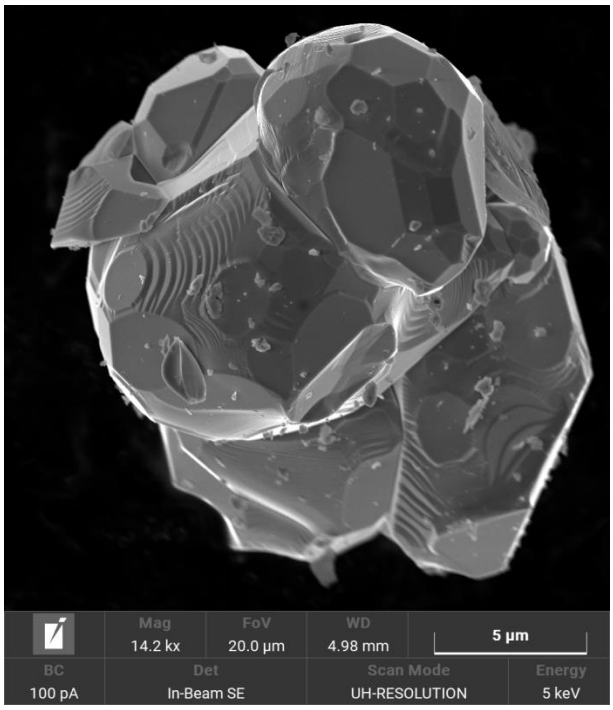

Fig. S7: FESEM image of (Co,Mg,Mn,Ni,Zn)(Al,Co,Cr,Fe,Mn)$_2$O$_4$. Image collected at 5 kV with the In-Beam SE detector. Instrumental magnification: 14200×.

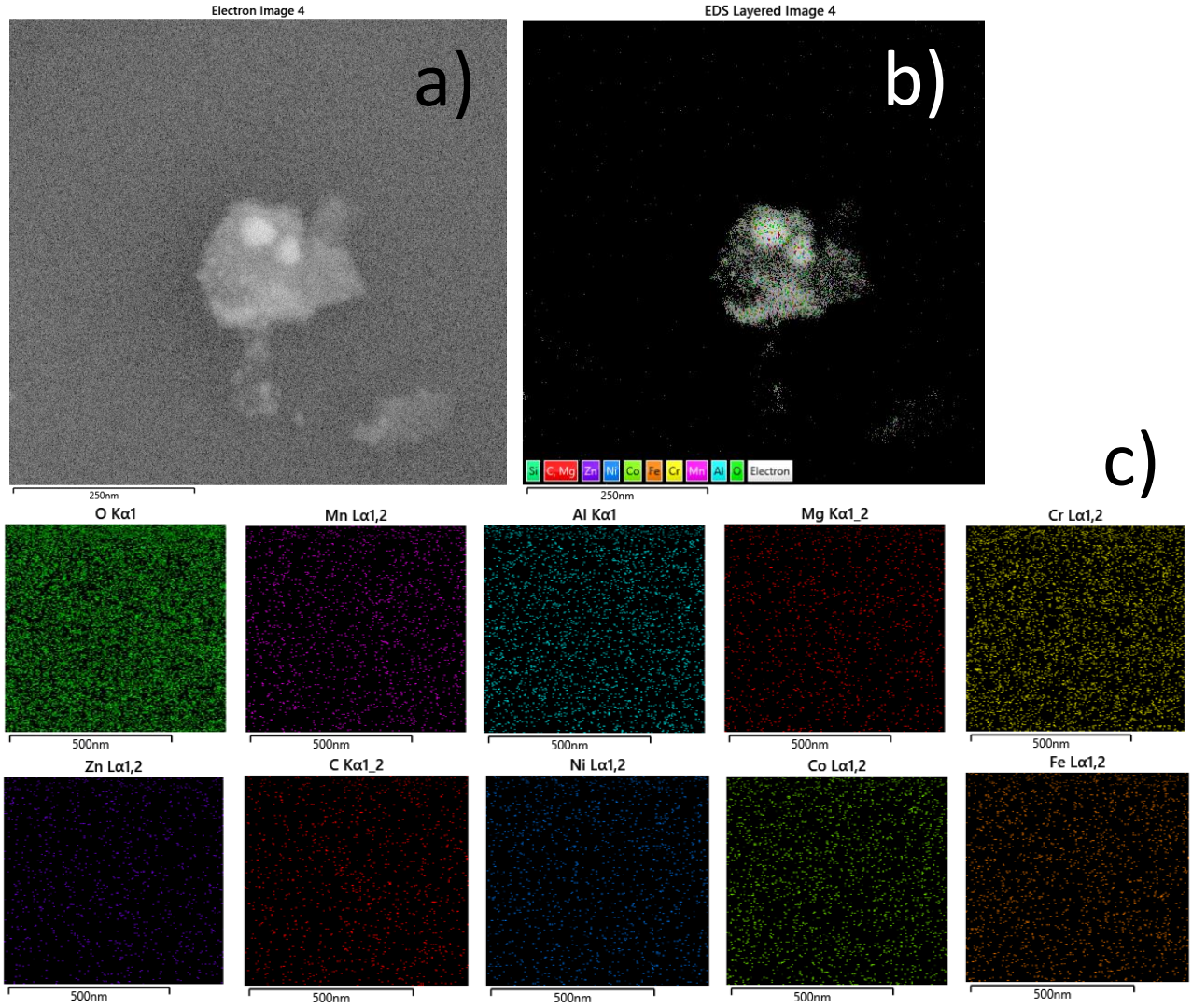

Fig. S8: a) FESEM image and b) EDS layered image of (Co,Mg,Mn,Ni,Zn)(Al,Co,Cr,Fe,Mn)$_2$O$_4$. c) EDS maps of the region shown in a) for all the 8 cations, oxygen (and carbon) in the spinel phase. Image collected at 25 kV with the standard SE detector. Instrumental magnification: 310000×.

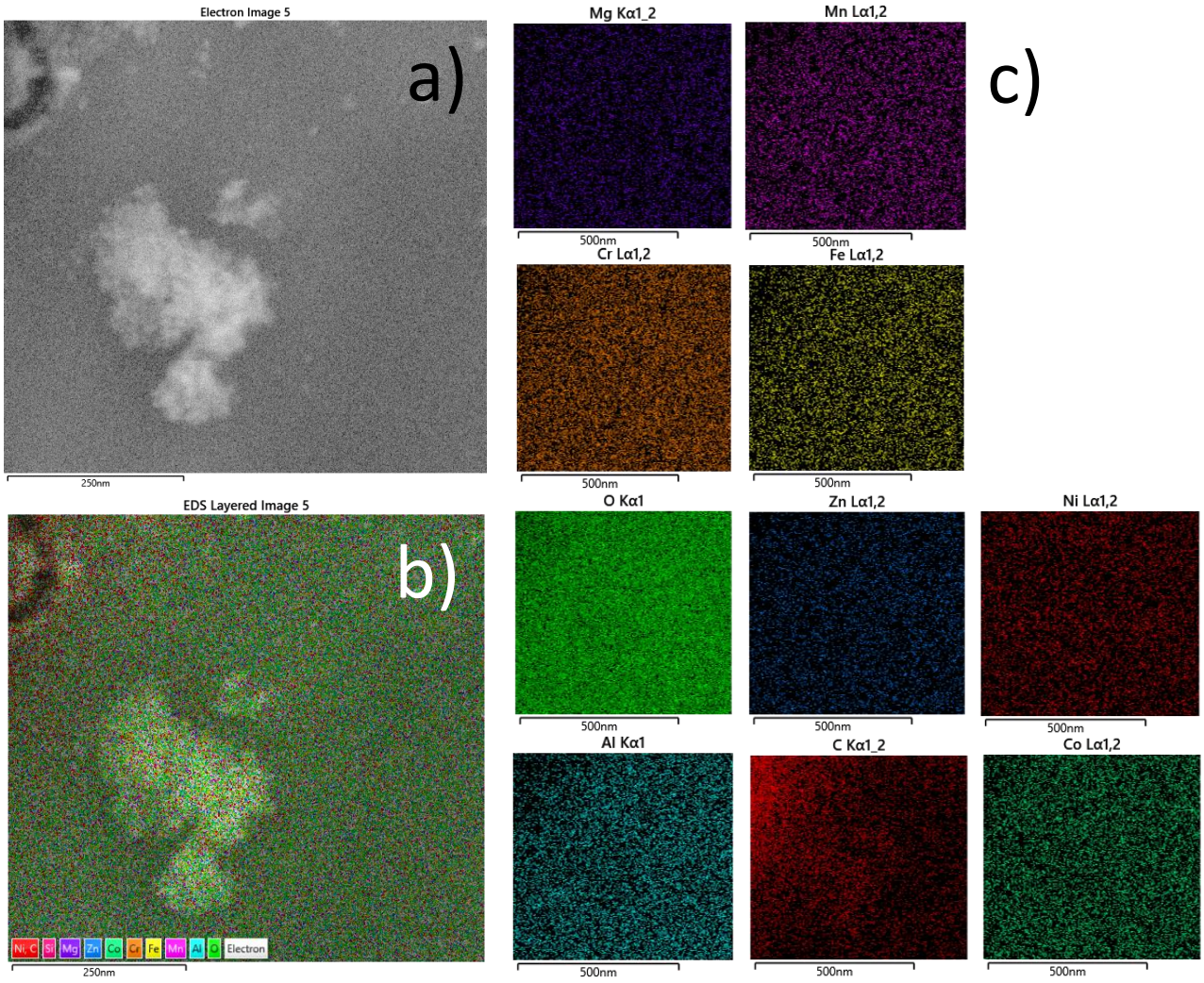

Fig. S9: a) FESEM image and b) EDS layered image of (Co,Mg,Mn,Ni,Zn)(Al,Co,Cr,Fe,Mn)$_2$O$_4$. c) EDS maps of the region shown in a) for all the 8 cations, oxygen (and carbon) in the spinel phase. Image collected at 25 kV with the standard SE detector. Instrumental magnification: 310000×.

X-ray Absorption spectroscopy (XAS)

The XAS spectra were measured at the XAFS beamline operating at the Elettra synchrotron radiation facility in Trieste, Italy [1]. The spectra were acquired at room temperature at the Co, Mn, Ni, Zn, Fe and Cr K-edge in transmission mode. The ring current and energy were 200 mA and 2.4 GeV, respectively. A Si(111) double crystal monochromator was used ensuring high-order harmonic rejection by de-tuning of the second crystal and a water cooled Pt-coated silicon mirror was used to obtain vertical collimation of the beam. For the measurements, a proper amount of sample (as to give a unit jump into the absorption coefficient) was mixed with cellulose and pressed into a pellet. The signal extraction was performed with the Athena code, belonging to the set of interactive programs IFEFFIT[2,3]. The pre-edge background was fitted by means of a straight line, while the post-edge by a cubic spline. All spectra were then normalized at unit absorption after the edge, where the EXAFS oscillations were no more visible.

For the fitting of the pre-edge peaks, the background due to the rising edge was simulated through a second-order polynomial function, and then subtracted to the experimental signal. The resulting curve was modelled using the minimum number of Gaussian functions.

[1] A. Di Cicco, G. Aquilanti, M. Minicucci, E. Principi, N. Novello, A. Cognigni, L. Olivi, J. Phys. Conf. Ser. 190 (2009).

[2] B. Ravel, M. Newville, J. Synchrotron Radiat. 12 (2005) 537–541.

[3] M. Newville, J. Synchrotron Radiat. 8 (2001) 322–324.